Tellus (1998), 50A, 507–524
Printed in UK – all rights reserved

TELLUS
ISSN 0280–6495

A hydrodynamic model of a quasi-steady two-dimensional front

By E. MOROZOVSKY*, G. I. BURDE, L. N. GUTMAN and A. ZANGVIL, *Meteorology Unit, Jacob Blaustein Institute for Desert Research, Ben-Gurion University, Sede-Boker Campus, 84990, Israel*

(Manuscript received 19 August 1997; in final form 25 February 1998)

ABSTRACT

A hydrodynamic model of a meteorological front has been constructed. This model is applicable to mature fronts which do not experience any conspicuous changes in intensity and shape and progress with approximately constant speed. The model considers cold and warm air masses, which are in contact along an interface and move above the horizontal earth under the influence of a given geostrophic wind. The closed-form solution of the problem incorporating (to a certain degree of approximation) the surface layer of atmosphere and allowing for the atmospheric turbulence has been obtained. On the basis of this solution, the global shape of the idealized frontal surface separating cold and warm air masses and the structure of the air flows in the vicinity of the front can be determined. The solution permits classification of mature fronts in terms of only two basic dimensionless parameters. The model is evaluated qualitatively by comparing some characteristics of the model with those observed for actual fronts. The comparison shows that the model provides a rational basis for interpreting observations and classification of fronts.

1. Introduction

Many investigations have been published which deal with frontal structure and evolution, including observations, theoretical and numerical studies (see e.g., reviews by Hoskins, 1982, Orlanski et al., 1985, Smith and Reeder, 1988). Most theoretical and numerical work has concentrated on the problem of frontogenesis. Williams (1967, 1972) has shown numerically using a primitive equation model that discontinuous fronts can form within a finite period of time if no turbulent diffusion is present. A two-dimensional version of the geostrophic momentum approximation introduced by Eliassen (1948) and first used by Sawer (1956) and Eliassen (1959, 1962) (referred to as the semigeostrophic equations) was successfully applied by Hoskins and Bretherton (1972) in their study of two-dimensional frontogenesis dynamics; see Hoskins (1982) for a review of semigeostrophic frontogenesis development. More recently, particularly illuminating have been the studies of frontogenesis in the presence of small moist symmetric stability by Emanuel (1985), Thorpe and Emanuel (1985) and Emanuel et al. (1987).

The structure of an atmospheric front as described by the semigeostrophic frontogenesis model has recently been tested against observational data by several authors (Blumen 1980; Ogura and Portis 1982). In summary, qualitative agreement was found in the details of the horizontal wind and temperature fields but major discrepancies were evident in the details of the vertical frontal circulation itself. In particular, the model was unable to reproduce an observed vertical velocity maximum near the surface. An under-

* Corresponding author.

standing of such cross-stream frontal circulation is important, not only because of its relevance to the basic dynamics of the frontal system, but also because of its role as a triggering mechanism for mesoscale convective phenomena such as prefrontal squall lines. The Hoskins and Bretherton solutions being successful in explaining frontal formation, continue only up to the initial formation of a discontinuity — at this stage frontogenetic effects dominate frontolytic effects. Observed frontal zones reach a finite, steady-state intensity as the frontogenetical geostrophic deformation patterns and frontolytical processes reach a balance (Browning et al., 1970). Observations of mature fronts, for instance those described by Sanders (1955), also show a balance between the effects.

It is expected that a dynamic balance, which characterizes mature fronts, can be achieved by including the turbulent diffusion into a model. Williams (1974) considered the generation of a steady-state circulation by including diffusion effects in a numerical model of a developing front that was produced by a deformation field. Also, simplified dynamic models with idealized initial conditions (Hoskins and West 1979; Blumen 1990) indicate that dissipation and surface friction are required to offset frontogenetic terms and thereby to produce a balanced state.

Eliassen (1959) pointed out the importance of surface friction in enhancing ageostrophic vertical flow. Blumen (1980) and Blumen and Wu (1983) introduced an Ekman layer into the Hoskins–Bretherton model to improve the vertical velocity field. Keyser and Anthes (1982) in their simulation of frontogenesis on the basis of numerical solution of primitive equations found that a frictionally driven ageostrophic boundary layer inflow was responsible for the creation of a vertical jet ahead of the surface front. Thompson and Williams (1997) studying the impact of boundary layer processes on maritime frontogenesis found that in the adiabatic and inviscid case simulation, strong warm and cold fronts formed but the vertical motion fields were weak; in the K-theory simulation, results were somewhat more realistic with stronger vertical motion.

Thus there are strong indications that including effects of surface friction and turbulent momentum diffusion is obligatory to obtain a correct picture of the circulation within a fully developed front. At the same time the attempts to resolve the disagreements with observations by adding frictional effects in simplified frontogenetic models were not very successful. Consequently there is an incentive to consider a mature front model excluding frontogenetic forcing effects but including instead some other factors, like surface friction and turbulent momentum diffusion, which affect the circulation within a mature frontal system.

There exist a number of mature front models, which consider the front as a surface of discontinuity between cold and warm air masses in a stationary or steady motion state ("balanced air mass theories" according to the terminology of Smith and Reeder 1988). We do not consider the gravity current models (see, e.g., Simpson, 1982), since the Coriolis force is absent in these models, their applicability to real fronts is restricted by the small scales. Some of the "balanced air mass" models include in one or another way the surface friction and/or turbulent friction effects.

Welander (1963) included diffusive effects in the well-known Margules (1906) model of a stationary front. However, he restricted himself to obtaining a special similarity solution for the frontal region, which does not satisfy the conditions at infinity so that the complete solution is lacking.

The frictional effects have been partially included in the model by Ball (1960) who developed a simplified formulation of a one-dimensional, stationary front (in the framework of shallow water theory) using a linearized bulk drag law. It appeared that the nonlinear terms in the horizontal equations of motion, in the approximation of shallow water theory and in a coordinate system moving with the front, are identically equal to zero if the mass flow beneath the front is zero as in the case when the front touches the ground. Theoretically possible shapes of frontal surfaces obtained in Ball's linear theory look plausible. Ball suggested a classification of fronts based on the frontal surface shape. Some extension of Ball's theory made by including the variable geostrophic wind field in the model was developed by Manton (1985).

In the works of Gutman and Mal'ko (1961) and Kalazhokov and Gutman (1964) the internal friction effects were included in a model of the planetary boundary layer consisting of cold and warm air masses by employing a constant eddy viscosity coefficient. The authors, guided by a

success of Ball's (1960) linear theory, used linearized horizontal equations of motion in the more general problem formulation: the two-dimensional equations are solved instead of the shallow water equations, and both the frontal surface shape and horizontal and vertical velocity fields are determined in the course of solution.

Rao (1971) constructed the numerical model which like the Kalazhokov and Gutman (1964) model is based on the linearized planetary boundary layer equations of motion but the vertical coefficient of turbulent viscosity is permitted to vary spatially with height. As distinct from the Kalazhokov and Gutman model, the shape of frontal surface is not determined in the process of solution but imposed in the form of an inclined plane with a given slope. It is important to emphasize that a comparison of the results with observational data for the specific examples of fronts shows that the consideration of the linearized front problem is sound and promising.

The formulation of the problem in Egger (1988) in main features coincides with that of Kalazhokov and Gutman (1964), though Egger considered the only particular case — the stationary front. However, in contrast to the work of Kalazhokov and Gutman (1964) and other aforementioned works, the formulation of the problem in Egger (1988) requires the vertical velocity to damp with height in the warm air mass. Since this problem is formulated as one of the boundary layer type (the hydrostatic equation is applied instead of the vertical equation of motion, which reduces the order of equations with respect to the vertical coordinate), this condition overdetermines the problem. As a result, the geostrophic wind, which sets the system in motion and therefore is the external parameter of the problem, becomes a function of the horizontal coordinate to be determined. Another distinction of Egger's work is that, in addition to the no-slip condition at the earth used in Kalazhokov and Gutman (1964), the case of a bulk formula for stress as the boundary condition is considered and these two variants of calculations are compared.

We will mention also the work by Manton (1981) who included into the inviscid frictionless model of a steady-state front the horizontal density gradients and the variability of the along-front component of geostrophic wind. This model gives a variety of possible streamline configurations, many of which are not expected to occur in practice. At the same time the model cannot yield, for example, solutions with a positive interface curvature which are seemingly relevant to conceptual models of anafronts taken from observations (see, for example, Browning 1986).

The aforementioned studies indicate that including the surface friction and the internal friction effects into "balanced air mass theories" are of importance in such models of steady-state mature fronts. Nevertheless, there were no models incorporating both effects in a non-contradictory way.

In the present work we try to introduce into the problem of a steady-state front a simple model of the surface layer, while retaining the principal features of the statement of the problem from the aforementioned works of Gutman and his collaborators. The two-dimensional, hydrostatic, linear model containing the parameterizations of the surface layer and vertical turbulent momentum diffusion considers a stationary or steady translating front as a discontinuity between two air masses having different but uniform temperatures. Thus both frontogenetic effect of the geostrophic wind shear and frontolytic effect of thermal diffusion are removed from the model. This justifies to a certain degree the use of the linearized equations, which provides an analytical representation of the solution. Although this simplified model corresponds to a highly idealized approach to the problem, it, as shown below, appears to capture the main features of the circulation within a mature frontal system, some of which are not seen in semi-geostrophic frontogenesis models.

2. Formulation and solution of the problem

2.1. Formulation of the problem

Consider the motion of air in cold and warm air masses in contact along a frontal surface (the shape of the surface is not known in advance); this surface we shall call "front" for brevity. An idealization of a transition (inversion) layer between cold and warm air masses as a discontinuity is partially justified by the fact that the vertical and horizontal dimensions of the region of frontal motion are much larger than the thickness of this layer. The entire system propagates horizontally under the action of both the external large-scale

(geostrophic wind) and the thermally induced pressure fields.

The following assumptions are made.

(1) The potential temperature of each of the air masses is known and constant (there is no diffusion of temperature across the interface). This assumption neglects the influence of the dynamical processes on the temperature field in each air mass, but it is important that the principal factor characterizing the frontal dynamics, namely the difference between the temperatures of the air masses, is taken into account.

(2) The front is propagating horizontally at a constant velocity without changing shape and its shape does not vary in the direction perpendicular to the front's movement. In the coordinate system moving with the front the process is considered as a steady-state.

(3) The geostrophic wind is given, non-zero and constant in space and time. The wind in the warm air mass is required to tend with height to the geostrophic wind.

(4) The characteristic inclination of the front is small, as indeed takes place in nature, which implies that the characteristic horizontal scales of the frontal motions are considerably larger than their vertical scales (see below the scales chosen for dimensionless variables).

(5) The quasistatic equation can be applied instead of the vertical equation of motion. This simplification is justified by the previous assumption.

Note that these five assumptions are, more or less, common for all the steady-state mature frontal theories reviewed in the Introduction.

(6) We will assume that there exists a neutral logarithmic surface layer of a given and constant thickness. The surface of the earth is assumed to be of uniform roughness. We neglect divergence and convergence of air in the surface layer — one can show that the error is of the same order as the ratio of the thickness of the surface layer to the characteristic vertical scale of the problem ($<10\%$); such an error is permissible in our idealized problem.

(7) The turbulent field in both air masses above the surface layer is described by the given constant turbulence coefficient.

(8) In the horizontal equations of motion, following the approach of Gutman and Kalazhokov (1964) and Rao (1971), we neglect the non-linear terms. The nonlinearity playing an important role in the processes of frontogenesis is presumably less important in the problem of a mature steady front, the more so as the processes in a transition zone between cold and warm air masses are out of consideration since it is replaced by an interface. The linearization is also justified to a certain degree by the success of Ball's (1960) linear one-dimensional theory. Note that a retrospective estimate of the nonlinear terms on the basis of the solution obtained (see Section 4) shows that in many cases the linearization is quite acceptable.

(9) In the continuity equations the decrease of air density with height can be omitted. One can show (Gutman 1972) that for heights lower than 3 km such neglect is permissible. Some errors appear at higher altitudes.

Proceeding to the mathematical formulation, we use a right-handed Cartesian coordinate system (x, y, z) with horizontal x- and y-axes (in the northern hemisphere y will lie to the left of x) and vertical z-axis. Confining ourselves to consideration of the front, which touches the ground, we place the origin of coordinates on the front, on the upper boundary of the surface layer, so that the system of coordinates moves together with the front. The line of intersection between the front and the upper boundary of the surface layer we call the surface front. A schematic picture of the model for the case of a cold front is presented in Fig. 1. The following notation is used: $z = h(x)$ is the equation for the front; z_s (const) is the given thickness of the surface layer; the number 1 and 2 indicate that further the tagged values relate to the cold and warm air masses, respectively. The x-axis is chosen to be normal to the front, its direction being defined either by the direction of frontal propagation (if the front velocity $c \neq 0$), or by the direction of the x-component of the geostrophic wind (if $c = 0$). In the special case where $c = u_g = 0$, it should be directed in such a way that the y-component of the geostrophic wind v_g is positive. We restrict ourselves to considering fronts for which

$$c \geqslant 0,\ u_g \geqslant 0 \quad -\pi/2 < \alpha < \pi/2, \tag{1}$$

where $\alpha = -\arctan(v_g/u_g)$ is the angle of inclination of the front velocity vector with respect to

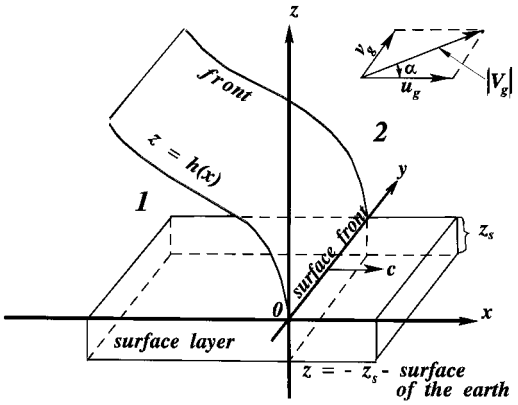

Fig. 1. Sketch of the model. The geostrophic wind is shown on the upper right; $z = h(x)$ is the equation for the front; z_s is the given constant thickness of the surface layer; the numbers 1 and 2 are related to the cold and warm air masses, respectively.

the direction of geostrophic wind. To the authors' knowledge there is no evidence in the literature that fronts moving against geostrophic wind exist.

Simplifying the quasistatic equation in view of the smallness of perturbations of the air temperature, pressure and density and then integrating this equation with respect to z while allowing for the common condition of pressure continuity at the front, one obtains:

$$p_1 = \rho_0 g\theta(h - z)/\Theta_0, \quad p_2 = 0, \tag{2}$$

where p_1 and p_2 are the pressure perturbations, θ is the constant potential temperature difference between the warm and the cold air masses, Θ_0 (const) is the given mean potential temperature of the atmosphere, g is the acceleration of gravity, and ρ_0 (const) is the mean density of the atmosphere. Inserting p_1 and p_2 from (2) into the linearized horizontal equations of motion we arrive at the equations, which in complex notation may be written as follows:

$$K\frac{\partial^2 V_j}{\partial z^2} - if(V_j - V_g) = (2-j)\frac{g\theta}{\Theta_0}h' \quad (j = 1, 2),$$
$$(V_j = u_j + iv_j, \quad V_g = u_g + iv_g, \quad h' = \mathrm{d}h/\mathrm{d}x). \tag{3}$$

Hereafter the quantity j (whether subscript or number) may take two values: $j = 1$ and $j = 2$. The rest of the notation is as follows: K is a given constant turbulent exchange coefficient, f (const) is the Coriolis parameter, and $u_j(x, z)$, $v_j(x, z)$ are the horizontal wind components.

The continuity equations are written as follows

$$\frac{\partial u_j}{\partial x} + \frac{\partial w_j}{\partial z} = 0, \tag{4}$$

where $w_j(x, z)$ are the vertical wind components.

Written in complex form, the equation for the wind velocity in the surface layer is:

$$V_s = \frac{V_*}{k}\ln\left(1 + \frac{z_s + z}{z_0}\right), \quad -z_s \leqslant z \leqslant 0,$$
$$(V_s = u_s + iv_s, \quad V_* = u_* + iv_*), \tag{5}$$

where $u_s(x, z)$ and $v_s(x, z)$ are the wind components in the surface layer, $u_*(x)$ and $v_*(x)$ are the components of the friction velocity, k is Von Karman's constant, and z_0 (const) is the given roughness length. It should be emphasized that all the wind and friction velocities in eqs. (3), (4) and (5) are measured relative to the ground.

Let us now show (see also Panofsky and Dutton 1984) that in the first approximation the introduction of the surface layer (5) into the problem can be reduced to modifying the boundary condition for V_j at $z = 0$. Assuming that at the upper boundary of the surface layer, wind velocity and its derivative with respect to z are continuous, we have the following matching conditions

$$V_s = V_j, \quad \frac{\partial V_s}{\partial z} = \frac{\partial V_j}{\partial z} \quad \text{at } z = 0. \tag{6}$$

It should be noted that these conditions do not provide continuity for the turbulent stresses at $z = 0$ but it does not introduce an additional error in the problem since some simplifying assumptions concerning the turbulent field ($z_s = \text{const}$ and $K = \text{const}$) have already been made. Substituting V_s from (5) into (6) and eliminating V_*/k, we obtain the condition:

$$V_j = b\frac{\partial V_j}{\partial z} \quad \text{at } z = 0, \tag{7}$$

where

$$b = (z_0 + z_s)\ln\frac{z_0 + z_s}{z_0}. \tag{8}$$

Thus, in our model the effect of the surface layer manifests itself only via parameter b. Setting $z_s = 0$ in (8) yields $b = 0$ and (7) is converted into the usual no-slip condition.

Table 1. *Scales chosen for the non-dimensionalization of the problem*; the bottom row gives numerical values of scales calculated for $K = 10\ \mathrm{m^2\ s^{-1}}$, $\theta = 10$ K, $\Theta_0 = 300$ K, $V_g = 10\ \mathrm{m\ s^{-1}}$, $f = 10^{-4}\ \mathrm{s^{-1}}$ and $g = 10\ \mathrm{m\ s^{-1}}$

Values	z, h	x, y	u_j, v_j, V_j	w_j
Scales	$\left(\frac{2K}{f}\right)^{1/2}$	$\frac{g\theta}{\Theta_0 f\lvert V_g\rvert}\left(\frac{2K}{f}\right)^{1/2}$	$\lvert V_g\rvert = (u_g^2 + v_g^2)^{1/2}$	$\frac{\Theta_0 f\lvert V_g\rvert^2}{g\theta}$
Estimations of scales	450 m	150 km	10 m/s	3 cm/s

To make the problem non-dimensional we choose the scales presented in Table 1. The equation of motion (3) rewritten in dimensionless form is:

$$\frac{\partial^2 V_j}{\partial z^2} + 2i(e^{-i\alpha} - V_j) = (2-j)2h'. \tag{9}$$

Hereafter we will adhere to the same notation for the dimensionless variables. The continuity equation (4) remains the same in non-dimensional form.

The dimensionless boundary conditions are:

$$V_j = B\frac{\partial V_j}{\partial z}, \quad w_j = 0 \quad \text{at } z = 0, \tag{10}$$

$$\left.\begin{aligned} V_1 = V_2, \quad \frac{\partial V_1}{\partial z} = \frac{\partial V_2}{\partial z}, \\ w_1 = w_2 = (u_1 - C)h' \end{aligned}\right\} \text{ at } z = h, \tag{11, 12}$$

$$V_2 = e^{-i\alpha} \quad \text{at } z = \infty, \tag{13}$$

where we denote

$$B = b(f/2K)^{1/2}. \quad C = c/|V_g|. \tag{14}$$

To complete the mathematical formulation of the problem we integrate eq. (4) for $j = 1$ with respect to z from $z = 0$ to $z = h(x)$ and then with respect to x. Taking into account the second condition in (10), condition (12), and also an obvious condition

$$h = 0 \quad \text{at } x = 0, \tag{15}$$

(front touches the ground), we obtain the following result:

$$\int_0^{h(x)} (u_1 - C)\,dz = 0. \tag{16}$$

This equation means that the total air flux through any vertical cross section of the cold air mass moving with the front equals zero.

Some remarks concerning the formulation of the problem defined by eqs. (4), (9)–(13), (15) and (16) are needed.

In condition (10) at the top of the surface layer, the non-dimensional parameter B characterizes the influence of the surface layer. For the conventional values: $10^{-2}\ \mathrm{cm} \leqslant z_0 \leqslant 1$ m, $z_s = 50$ m and $(2K/f)^{1/2} = 500$ m, in accordance with eqs. (8) and (14) we have

$$0.4 \leqslant B \leqslant 1.3. \tag{17}$$

The fact that B is of the order of 1 shows that incorporating the surface layer in the problem would substantially affect the solution. The second condition in (10) is a result of neglecting divergence and convergence of air in the surface layer.

The conditions (11) of the wind continuity at the front are necessary since the turbulent friction has been included into the equations of motion. As distinct from the inviscid counterpart of the model (the Margules model), a jump of the wind at the frontal surface cannot exist, when the turbulent friction is present, and the wind, instead of being constant in each air mass, varies from the wind in the surface layer to the geostrophic wind. As a matter of fact, the system of equations (4) and (9) with the boundary conditions (10)–(13) replaces the thermal wind relation, or the Margules discontinuity relation, for the jump of the geostrophic wind. The second condition in (11) is written in a form that implies that the characteristic inclination of the front is small, as indeed takes place in nature.

The second condition in (12) expresses a well-known property of meteorological fronts, namely impermeability for regular airflows. As a matter of fact, in our formulation the front is a material surface and this is a kinematic condition at it. Note that although the problem is being considered in a coordinate system moving at the velocity

c, this quantity figures explicitly only in condition (12); this facilitates the solution of the problem.

The condition (13) requires the wind to tend with height to the geostrophic wind. It is important to emphasize that the hydrostatic approximation, made in the vertical equation of motion, reduces the order of equations with respect to the vertical coordinate (the problem becomes a boundary layer type problem) so that a reduction of the minimum essential boundary conditions is inevitable. Therefore one can not impose additional conditions at infinity, for example, a condition for the vertical velocity — it would overdetermine the problem. For the same reason a relation similar to (16) (mass flow continuity) could not be imposed for the upper flow — there is no condition for the vertical velocity component (and, in particular, it does not vanish) at the large distances from the surface.

Similarly, because of the absence of the horizontal diffusion terms in the momentum eqs. (9), one does not need lateral boundary conditions except the conditions (15) and (16) which specify the solution at $x=0$ and determine a further development of the solution (see the next section).

2.2. Solution

The solution of eqs. (9) can be written in the form:

$$\left.\begin{aligned} V_1 &= c_1\,\mathrm{e}^{(i+1)z} + c_2\,\mathrm{e}^{-(i+1)z} + \mathrm{e}^{-i\alpha} + ih', \\ V_2 &= c_3\,\mathrm{e}^{-(i+1)z} + \mathrm{e}^{-i\alpha}, \end{aligned}\right\} \tag{18}$$

where c_1, c_2 and c_3 are arbitrary complex functions of x. One can see that V_2 as given by (18) satisfies condition (13). The functions c_1, c_2 and c_3 obtained from conditions (10) and (11) are:

$$\left.\begin{aligned} c_1 &= -\frac{ih'}{2}\,\mathrm{e}^{-(1+i)h}, \quad c_2 = c_1 - n(\mathrm{e}^{-i\alpha} + ih' + 2c_1) \\ c_3 &= c_2 + \frac{ih'}{2}\,\mathrm{e}^{(1+i)h}, \quad (n = (i+1)\cos\beta\,\mathrm{e}^{-i\beta}) \end{aligned}\right\}. \tag{19}$$

Here instead of B a new parameter β appears:

$$\beta = \arctan(1+2B). \tag{20}$$

This substitution turns out to be convenient for our analysis. Thus, the effect of the surface layer now manifests itself in the problem via the parameter β. It follows from (17) and (20) that the values of the parameter range within a comparatively narrow interval:

$$1.1 \leqslant \beta \leqslant 1.3\,. \tag{21}$$

In view of the approximate nature of our idealized problem, in many cases (although not always) one can take for β the mean value 1.2.

We note that $\beta = \pi/4$ ($B=0$) corresponds to ordinary non-slip conditions at the ground (i.e., to absence of the atmospheric surface layer) and $\beta = \pi/2$ ($B=\infty$) corresponds to the absence of air friction at $z=0$. Both quantities lie outside the interval given by (21).

The solution given by (18) and (19) determines horizontal velocities u_j and v_j. Vertical velocities w_j are easily obtained from (18) and (19) with the help of the continuity equation, as follows:

$$w_j = -\frac{\partial \psi_j}{\partial z}, \quad \psi_j = \int_{(j-1)h}^{z} (u_j - C)\,\mathrm{d}z\,, \tag{22}$$

where ψ_j are streamfunctions defining streamlines of the stationary flow in the moving coordinate system.

All the expressions in (19) and (22) contain the unknown function $h(x)$ and its derivative $h'(x)$. To obtain an equation for $h(x)$, we substitute $u_1 = \mathrm{Re}\,V_1$ into (16). After integration and elementary transformations we arrive at the ordinary nonlinear first-order equation

$$h' = N/D\,, \tag{23}$$

where

$$D = \frac{\sec\beta}{4}\left[1 - \mathrm{e}^{-2h}(\sin 2h + \cos 2h)\right] + \sin\beta - 2\,\mathrm{e}^{-h}\sin(\beta + h) + \mathrm{e}^{-2h}\sin(\beta + 2h), \tag{24}$$

$$N = hA + \mathrm{e}^{-h}\cos(\gamma + h) - \cos\gamma\,. \tag{25}$$

Here, we denote

$$A = \frac{\cos\alpha - C}{\cos\beta} = \frac{u_{\mathrm{g}} - c}{|V_{\mathrm{g}}|\cos\beta}, \tag{26}$$

$$\gamma = \alpha + \beta \quad (-0.5 < \gamma < 2.9)\,. \tag{27}$$

The inequalities in brackets are derived from (1) and (21).

Thus, instead of C and α two new non-dimensional parameters A and γ now appear (see discussion of the physical sense of the parameters at the beginning of Section 3). The solution given by

eqs. (18), (19), (22) and (23)–(25) is determined by three parameters A, γ and β (the parameters α and C contained in (18), (19) and (22) can be expressed through A, γ and β).

It follows from eqs. (23)–(27) that so-called stationary fronts ($c=0$) do not stand out in our formulation of the problem, and therefore one does not need to consider stationary fronts separately. The condition that C cannot be negative (see (1)) combined with (26) and (27) imposes the following condition on the parameters

$$\cos\gamma + \tan\beta \sin\gamma \geqslant A\,. \tag{28}$$

Eq. (23) for the function $h(x)$ can be solved numerically with the boundary condition (15). The solution is used both in calculations of the wind velocities by (18), (19) and (22) and for determining a shape of the front. However, the following analytical investigation of the integral curves of this equation provides almost all the essential information related to shapes of fronts.

First, it is easy to show that for all β defined by (21), the denominator D in (23) is a monotone positive-definite function of h and $D=0$ only at $h=0$. Since $|N|<\infty$ for any $h<\infty$, one can conclude that a front can be vertical only at the point $h=0$ and that the sign of the frontal slope cannot change with height. The first term in the expansion of the ratio N/D for $h \ll 1$ into the power series of h can be found using (24) and (25), as follows

$$h' \approx -\frac{\cos\beta}{\cos 2\beta} \times \begin{Bmatrix} a/h, & \text{if } a \neq 0 \\ \sin\gamma, & \text{if } a=0,\ \gamma>0 \\ h/3, & \text{if } a=\gamma=0 \end{Bmatrix} \quad \left(\frac{\pi}{4}<\beta<\frac{\pi}{2}\right), \tag{29}$$

where

$$a = A - \sin\gamma - \cos\gamma\,. \tag{30}$$

The formulae (29) are not valid if $\beta=\pi/4$ — in this case $h' \approx (-3/2)Ch^{-2}$.

In what follows the special case of $a=0$ will be ignored and the study will concentrate on the general case of $a \neq 0$. Since the factor $(-\cos\beta/\cos 2\beta)$ in front of the brackets in (29) is positive for all β given by (21), the sign of h' coincides with the sign of a. This means that $a>0$ corresponds to warm fronts and $a<0$ — to cold fronts. It is seen from (29) that for $a \neq 0$, eq. (23) has a singularity at the point $x=0$, at which the boundary condition (15) must be satisfied. Thus, both cold and warm fronts cross the surface layer at a right angle and consequently the y-axes, which is at the same time the surface front, is the singular line of solution. In the vicinity of the surface front, our assumption that the horizontal scales of the process exceed the vertical scales is not fulfilled. Note that it is a typical situation in fluid dynamics problems and it is known that, outside this small area, the solution remains valid and is physically significant.

One can also derive from (23) some qualitative conclusions concerning the global behavior of the integral curves $h(x)$. It depends on whether the transcendental equation

$$Ah_1 = \cos\gamma - \mathrm{e}^{-h_1}\cos(h_1+\gamma), \tag{31}$$

obtained by setting a numerator $N=0$ in (25) has at least one real root h_1 (if there are several real roots, one must take the smallest of them as h_1). In the case when h_1 exists, the front approaches the height h_1 asymptotically, becoming horizontal. This occurs at $x=\infty$ for warm fronts and at $x=-\infty$ for cold fronts. Thus h_1 is actually the thickness of the cold air mass. It easy to show that h_1 exists if A satisfies the inequalities:

$$\cos\gamma + \sin\gamma > A > \begin{cases} 0 & \text{for } -\dfrac{\pi}{4}<\gamma<\dfrac{\pi}{2} \\ A_* & \text{for } \dfrac{\pi}{2}<\gamma<\dfrac{3\pi}{4}, \end{cases} \qquad 0 > A > A_* \quad \text{for } \frac{3\pi}{4}<\gamma<\pi\,, \tag{32}$$

where the function $A_*(\gamma)$ can be obtained from a system of two transcendental equations:

$$\begin{aligned} A_* h &= \cos\gamma - \mathrm{e}^{-h}\cos(\gamma+h)\,, \\ A_* &= \mathrm{e}^{-h}[\cos(\gamma+h)+\sin(\gamma+h)]\,. \end{aligned} \tag{33}$$

Outside the ranges set by inequalities (32), fronts must be of unlimited height. By solving equation (23) analytically for $h \gg 1$ one can show that, in the upper sections of such fronts, the height of the front increases exponentially with the exponent $|Ax/D_{h=\infty}|$ for both cold and warm fronts.

To find u_j, v_j, w_j and ψ_j, the function $h(x)$ obtained as the result of numerical integration of eq. (23) is substituted into (18), (19) and (22). This yields a solution for the area beneath and above

the front, i.e., for $x<0$ in the case of the cold fronts and for $x>0$ in the case of the warm fronts. To determine the form of the solution for the section $x=0$ one has to pass to the limit $h\to 0$ in (18), (19) and (23)–(25).

To conceive an approximate picture of the air motion in areas ahead of the cold front and behind the warm front, we use the following interpolation method. The solution for an area sufficiently remote from the surface front in the direction of the warm air mass can be obtained from (18) and (19) by setting $h=h'=0$ which corresponds to Ekman's well-known solution, complicated, if $\beta>\pi/4$, by the presence of the surface layer. Approximate pictures of the fields of wind velocity, vertical velocity and streamlines for the area $-L<x<0$ in the case of a warm front and for the area $0<x<L$ in the case of a cold front (here L is a horizontal distance at which the influence of the front on the air motion can be neglected) were computed by interpolation with use of cubic spline functions. The value of L was ascribed in each case on the basis of a rough physical estimate. The calculations showed that the results depend only to a slight extent on the specific value of L. For instance, the topological structure of the streamlines and isopleths does not depend on the value of L at all. Nevertheless, the specific value of L is indicated for each example of calculations presented below.

3. Classification of fronts

3.1. Frontal types

The solution presented in the previous section can be used to suggest a classification of front types. It is seen from the solution (Subsection 2.2) that the principal characteristics of the front related to its shape are determined by only two dimensionless parameters A and γ; it is sufficient to know these parameters to define whether a given front is cold or warm, shallow or deep. Asymptotic analysis of eqs. (18), (19) and (22) shows that also important flow features (for example, those defining whether it is an anafront or katafront) depend on the values of the parameters A and γ only. Thus, we have good reason to consider A and γ as parameters, which determine the type of front. It is useful for the following interpretation of the results to extract from the definitions (26) and (27) of A and γ some basic quantities. The parameter A should be thought of as a scaled difference between the front-normal geostrophic wind component u_g and the frontal speed c while the parameter γ is the angle between the front velocity and geostrophic wind vectors corrected by an "effective surface friction angle" β.

The parameter β plays a secondary part in our classification. It does not mean, however, that the value of this parameter is unimportant in the problem formulation and solution. Since the values of β estimated by (21) differ considerably from the value of $\pi/4$ corresponding to the absence of the surface layer, a number of essential frontal features, in particular, new frontal types, appear (see discussion below). The correction factors depending on β included in the parameters A and γ are also important as they considerably shift the values of these parameters determining the type of the front. At the same time *changes* in the value of β do not strongly influence the frontal type since they are confined within a rather narrow interval (21) and many properties of frontal motion are not very sensitive to a specific value of β from this interval.

A chart of frontal types on the Cartesian coordinate plane (A,γ) is presented in Fig. 2; some auxiliary information concerning the chart is presented separately in Fig. 3 in order not to overload the former figure. The pictures embedded in the chart in the Fig. 2 represent schematics of the front shapes and flow patterns in the vertical cross-sections normal to the front and moving with it. The calculated flow patterns corresponding to each front type are presented in Fig. 4 and are discussed below.

The following three thick lines: sinusoid $a=A-\sin\gamma-\cos\gamma=0$, straight line $A=0$ and the curve defined by (32) separate on the chart five domains (I, I′, I″, II, II′), which correspond to different types of fronts (Section 2). Below the sinusoid, in the area where $a<0$, domains corresponding to cold fronts are situated (I, I′ and I″). The area above the sinusoid ($a>0$) is occupied by domains corresponding to warm fronts (II and II′). According to (32) the domains I and II are domains of deep fronts while I′, I″ and II′ correspond to shallow fronts. Following Ball (1960) we refer to fronts whose height is limited by some value h_1 x(even though $h_1>1$) as shallow fronts and to fronts of unlimited height as deep fronts.

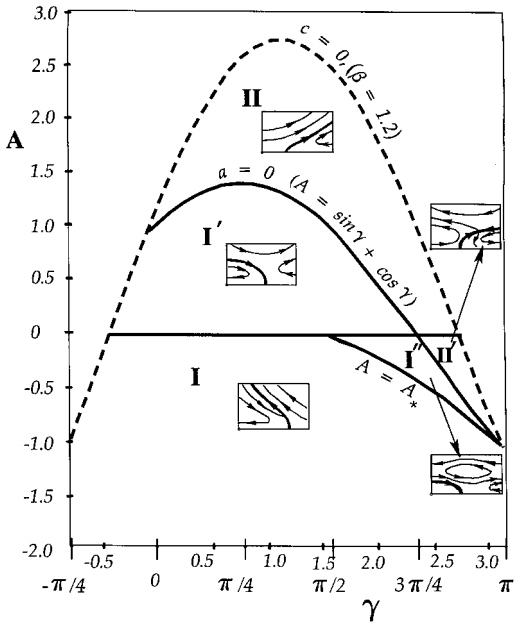

Fig. 2. Chart of the frontal types on the plane (A, γ). The heavy solid lines separate the domains of different types of fronts. The dashed line (plotted for $\beta = 1.2$) represents the upper boundary of the chart. The domains are numerated with Roman numerals and correspond to classification presented in Fig. 4. The pictures embedded are schematics of the streamline patterns (thin lines) and frontal shapes (thick lines) for each type.

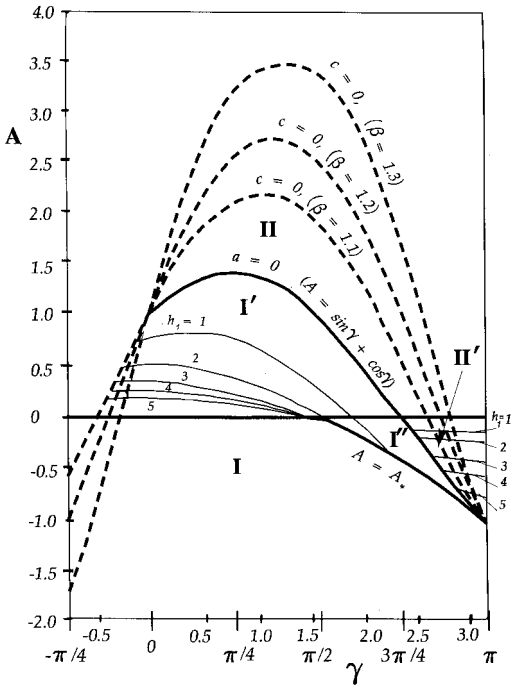

Fig. 3. The upper boundary of the chart for different β (dashed lines) and isolines of the dimensionless initial thickness of a cold air mass h_1 (thin solid lines).

For the domains of shallow fronts, thin solid lines in Fig. 3 draw isolines of the dimensionless initial thickness of a cold air mass h_1.

The upper boundary of the chart is determined by (28) which gives the upper limit for A as the sinusoid $A = \cos\gamma + \tan\beta \sin\gamma$ with the amplitude depending on β (the upper boundary shown by a dashed line in Fig. 2 corresponds to $\beta = 1.2$). Three sinusoids corresponding to $\beta = 1.1$, 1.2 and 1.3 are shown by dashed lines in Fig. 3. For a given β, fronts associated with the points of the limiting sinusoids are stationary ($c = 0$).

If $\beta = \pi/4$ the dashed curve coincides with the line $a = 0$. It means that, without allowance for the surface layer, the solutions corresponding to warm fronts, which touch the ground, do not exist at all in the model. It is an additional confirmation for the fact that the surface layer plays an important part in the model of front. If $\beta = \pi/2$ the dashed curve will degenerate into two straight lines: $\gamma = 0$ and $\gamma = \pi$.

We constructed, on the basis of the solution obtained, front shape and streamlines in (z, x) coordinate system (i.e., in the vertical cross-sections perpendicular to the front and moving with

Fig. 4. Classification of fronts. Exampless of each frontal type have been calculated for the following points of the chart: (I) $A = -0.3$, $\gamma = 0.5$; (I′) $A = 0.2$, $\gamma = 0.5$; (I″) $A = -0.2$, $\gamma = 2.3$; (II) $A = 0.3$, $\gamma = 2.5$; (II′) $A = -0.1$, $\gamma = 2.6$ ($\beta = 1.2$, $L = 6$ for all the cases). It is implies that fronts move from left to right in all 5 pictures. Every pattern is bounded from below by the upper boundary of the surface layer. Thick lines show the front shape; thin solid lines are streamlines in the vertical cross-section perpendicular to the front and moving with it; dashed lines are additional streamlines showing weak circulation in cold air; arrows show the flow direction relative to front. Horizontal and vertical coordinates and stream-function values are dimensionless.

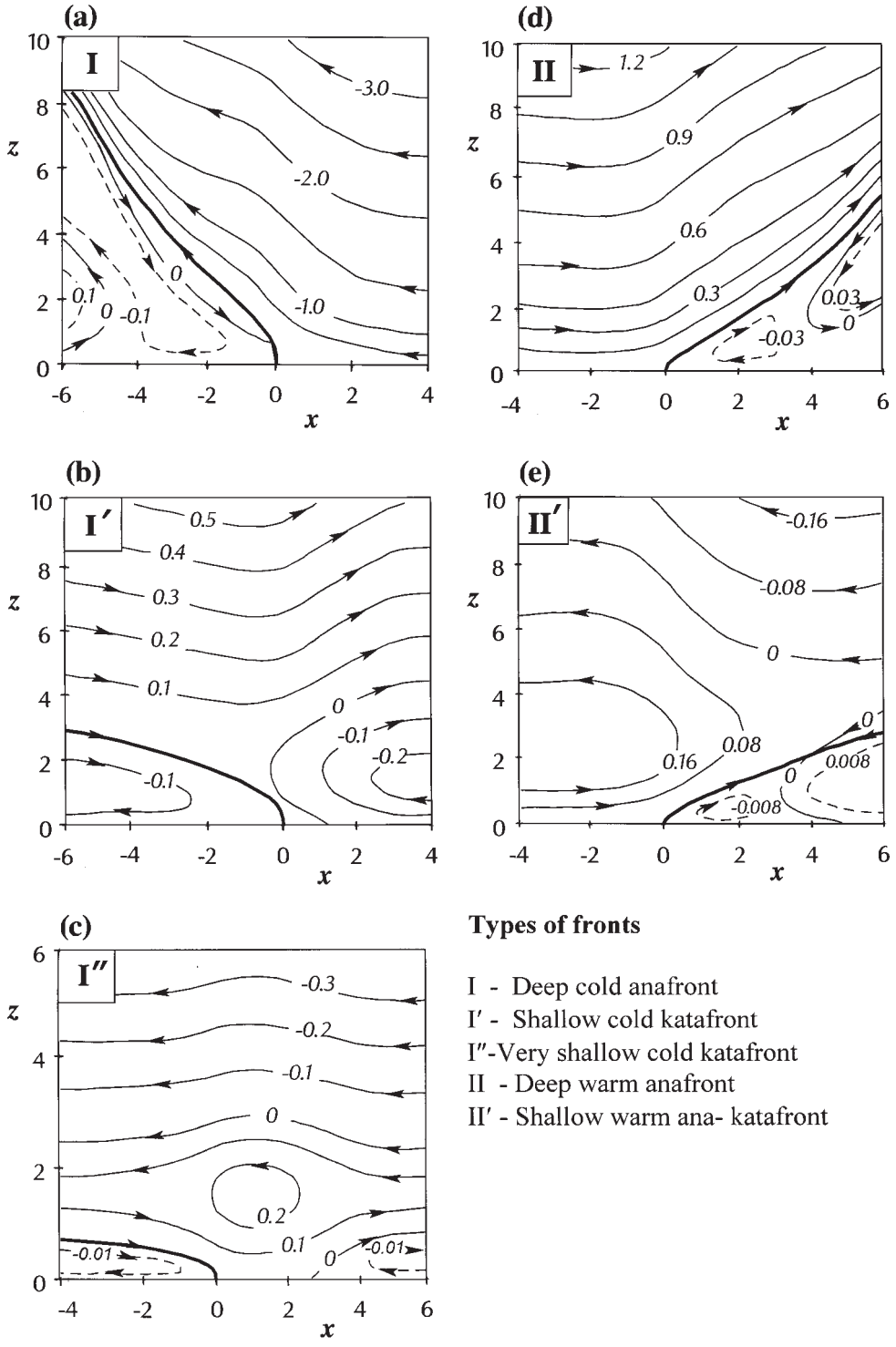

Types of fronts

I - Deep cold anafront
I′ - Shallow cold katafront
I″-Very shallow cold katafront
II - Deep warm anafront
II′ - Shallow warm ana- katafront

Fig. 4.

it) for different points of each domain. As distinct from the front shape, the air flow structure, in general, depends on all three parameters of the problem A, γ and β and hence it is not determined completely by the point selected on the plane (A, γ). Nevertheless, it turned out that every domain can be associated with a certain type of air flow as well. A change of the third parameter β results in a shift of streamlines (a weak circulation in a cold air mass in the vicinity of the surface front can change direction as well), but it does not influence the main features of the air flow picture. Thus, one can elicit air flow pictures typical for every domain and use them to classify frontal types.

Five flow patterns corresponding to all possible front types are shown in Fig. 4, where front shapes and the cross-frontal flow streamlines, calculated for certain points from each domain, are presented. Although the information provided by the frontal shape and streamline patterns is sufficient for the

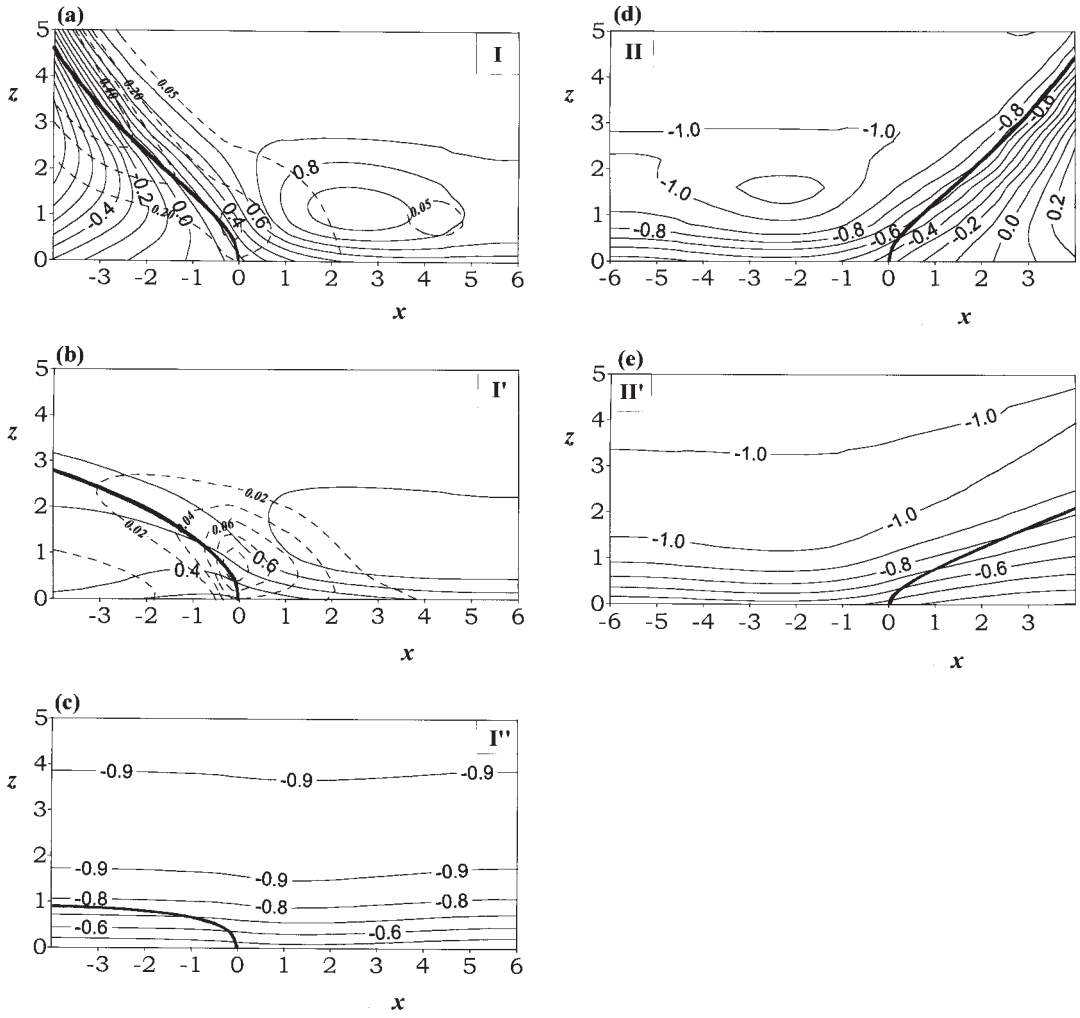

Fig. 5. Isopleths of the dimensionless along-front velocity $v = \text{const}$ corresponding to each type of front calculated for the same values of parameters A, β, and γ as in Fig. 4. The front (thick line) and isopleths of v (thin lines) are plotted in the vertical cross-section perpendicular to the front and moving with it. Dashed lines in (a) and (b) are selected isopleths of the quantity $u(\mathrm{d}v/\mathrm{d}x)/fu$ which is a measure of the relative magnitude of the neglected nonlinear terms.

presented classification, some additional features facilitating an identification of a frontal type in observational data can be seen in the fields of wind speed components u, v and w. The isopleths of the along-front velocity v, which are the most informative in a sense, are shown for each type of front in Fig. 5.

One can, in principle, find a qualitative physical explanation for the main features of stream-lines patterns and location of areas of ascending and descending air flows in Fig. 4. Evidently the main dynamic factors influencing the circulation patterns are the difference of geostrophic wind and frontal speed, the surface and internal turbulent friction and the Coriolis force. The direction of the flow above the front is mainly determined by the sign of the difference $u_g - c$. If $u_g < c$ ($A < 0$), the air aloft moves to meet the front and this, in the coordinate system moving with the front to the right, results in the flow above the front directed to the left. If, conversely, $u_g < c$ ($A > 0$) the air aloft runs down the front and the flow above the front in the moving coordinate system is to the right. The surface friction tends to make the flow near the ground directed to the left and the internal friction due to turbulent stresses tends to adjust the flow directions and velocities within the region. The interaction of all these factors produces, for example, such a ubiquitous feature of the cold katafront air flow (type I′) as a reversed flow ahead of the surface front, which results in a warm air ascent, and also causes the circulation of the cold air under the front. The interaction of the same factors in the case of the cold anafront (type I) results in a more complicated structure in which the narrow zone below the front, adjusting the upgliding flow direction above the front to the circulation near the ground, appears. Similar arguments are applicable for explaining the structure of the deep warm anafront air flow (type II).

The Coriolis force is evidently the factor responsible for an existence of the frontal types I″ and II′. These types of fronts occupy in Fig. 2 the area of large positive values of γ (or values of α of the order one and larger) and negative but small A which corresponds to negative and large values of v_g and negative and small values of $u_g - c$. The Coriolis force connected with v_g tends to cause the flow directed to the right which (because of a smallness of u-velocities produced by the difference $u_g - c$) can significantly reduce the flow velocity aloft and even reverse its direction below. Such a situation does not arise neither for small γ and negative A nor for large γ and positive A since in those cases the Coriolis force and the effect of the difference $u_g - c$ act in the same direction. The region of small γ and positive A is almost not included into the chart due to the restriction (28).

It should be noted that one could not pretend to explain all peculiarities of the cross-frontal circulation with the help of the above arguments. Complicated interaction of all the factors, which is described by the initial differential equations, may prevent a possibility of a qualitative explanation of the flow patterns in some regions (for example those at larger distances from the surface front) or some fine details of the flow. Nevertheless, the above considerations make the physical relations, which are responsible for some of the frontal features, easily understandable.

3.2. *Comparison with observations*

Three front types in our classification, namely, the types I, I′ and II, are well known from literature. Browning (1986) proposed conceptual models of precipitation systems, based on a broad observational data. The situation of "the warm conveyor belt with rearward sloping ascent" (see Fig. 3 in Browning 1986) actually coincides with the type I of our classification and corresponds to the classical cold anafront (see also the idealized picture of an anafront in Fig. 1A of Moor and Smith 1989). The characteristic feature of this type, besides the strong rearward ascending flow in a warm air mass above the front, is a narrow zone below the front in which a transition from ascending to descending flow occurs. As one can see from Fig. 4, this ubiquitous detail of the anafront airflow is well reproduced by our analytical solution.

Another peculiarity of type I fronts, which is known from observations, is detected by the analysis of the along-front velocity field: it is the horizontal low-level jet stream in the warm air mass which is parallel to the front and moves with it (see, for example, Browning and Pardoe 1973). The wind speed in the jet reaches sometimes few tens of meters per second; the jet axis is located at a distance of the order of 100 km ahead the surface front. The v-velocity fields calculated on the basis of our solution predict an appearance of

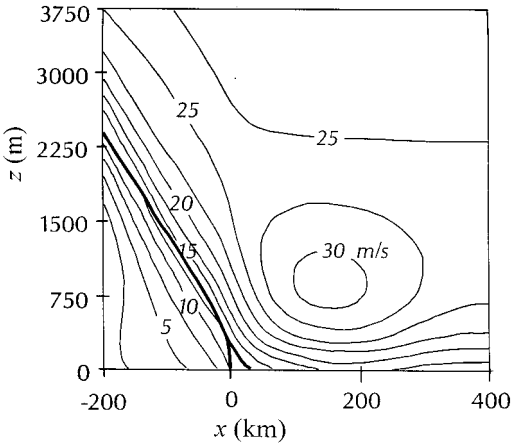

Fig. 6. An example of calculation of the front position (thick line) and isopleths along-front wind $v = \text{const}$ (thin lines) for the vertical cross-section perpendicular to the front and moving with it ($A = -0.2$, $\gamma = 0$, $\beta = 1.2$). The dimensional velocities and coordinates are calculated for the following values of parameters: $K = 28\ \text{m}^2\ \text{s}^{-1}$; $V_g = 25\ \text{m s}^{-1}$; $\theta = 7$ K.

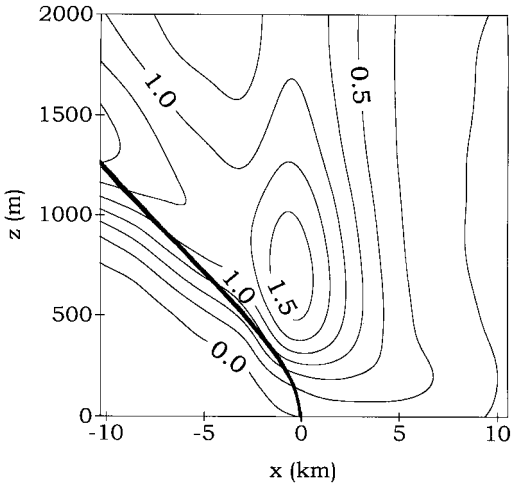

Fig. 7. An example of calculation of the front position (thick line) and isopleths of vertical velocity $w = \text{const}$ (thin lines) for the vertical cross-section perpendicular to the front and moving with it ($A = -1.0$, $\gamma = -0.1$, $\beta = 1.2$). The dimensional velocities and coordinates are calculated for the following values of parameters: $K = 12.5\ \text{m}^2\ \text{s}^{-1}$; $V_g = 30\ \text{m s}^{-1}$; $\theta = 3$ K.

a jet stream with similar characteristics if the non-dimensional parameters of the problem lie within a certain region of the domain I (see Fig. 5a). Browning and Pardoe (1973) also reported that the low-level jet streams were observed only ahead of cold anafronts. Isopleths of the v-velocity field for the values of dimensionless parameters and scales calculated on the basis of the data from Browning and Pardoe (1973) are presented in Fig. 6.

The vertical velocity field (Fig. 7) calculated on the basis of the data from the case-study by Bond and Fleagle (1985) shows that our model reproduces also a structure of the observed w-field and, in particular, a vertical velocity maximum near the surface.

A conceptual model of a cold katafront widely used in the literature (see, for example, Fig. 1B in Moor and Smith 1989) evidently corresponds to the flow structure of the type I′ fronts. This type also corresponds to "the warm conveyor belt with forward sloping ascent" situation described in Browning (1986) (see Fig. 4 of Browning 1986). The characteristic feature of this type is a warm air ascent ahead of the surface front with the subsequent turn of the flow in the vertical plane towards the direction of front movement.

The third type of front, which is well known to observational meteorologists, is a warm anafront appearing in our classification as the type II. It is easily seen, for example, that the transverse air circulation in the vicinity of a warm front, built on the basis of observational data in the work of Browning and Harrold (1969) (Fig. 10), looks to be very similar to the air flow of type II in Fig. 4. Note, that for this type (like for type I) there exists a narrow zone in which a transition from ascending flow above the front to descending flow below the front occurs. However, as distinct from the type I, here this zone is more narrow and does not reach the surface front. As a matter of fact, all the circulation in a cold air mass is so weak (the relative velocity component $u - c$ is small) that in most cases one can neglect this circulation and consider the cold air wedge (excluding the surface layer) moving as a solid.

We did not succeed in finding published observations, which could definitely confirm a realization in nature of the front types I″ and II′, though some observations could be interpreted in such a way. In any case the fronts of the types I″ and II′ should be observed much more rarely than the other three types since the domains I″ and II′ in

the chart are relatively small. Also it would be difficult to identify such fronts without detailed investigation of the air flow structure not only in the vicinity of the nose of the front but also at rather large distances from the front: it is easily seen from Fig. 4 that in the immediate vicinity of the surface front the type I″ looks like a common cold katafront I′ and the type II″ looks like a common warm anafront II. In addition the results of our model concerning a detailed structure of such shallow fronts as I″ (the thickness of the cold air mass $h_1 < 1$) are probably less reliable; for such fronts a hydrodynamic drag due to mixing at the head might be important in the force balance on the front. These fronts may pass unnoticed as well, because they should to a smaller degree than other fronts be associated with noticeable rain or wind, or any other conspicuous weather phenomena.

In conclusion of this section we will make two additional remarks. The first remark is about a comparison of the theoretical frontal shape with observations. Evidently, the type of the air flow in the vicinity of front should be a basic indication of the front type if one is trying to incorporate the observational data into a theoretical framework. The observational information concerning the frontal shape assumes certain meaning in statistical data because of the uncertainty that is inherent in a single observational analysis of the front (inversion) position. The most comprehensive study was made by Sansom (1951) who identified 50 cold fronts that crossed the British Isles as either anafronts or katafronts. His data show, in particular, that the mean slope of katafronts (1/300) is appreciably smaller than that of anafronts (1/70). This is in accordance with our solution in which the katafront flow structure is related to the frontal surface limited in the height (type I′) and the anafront flow structure is related to the unlimited frontal surface (type I) our model. Sansom (1951) indicated that in most cases increasing cyclonic or decreasing anticyclonic curvature takes place when crossing an anafront and on the contrary decreasing cyclonic or increasing anticyclonic curvature occurs for katafronts. That is also in agreement with the solution obtained: the sign of the additional curvature of isobars, connected with the pressure disturbance due to a front, is determined by the sign of d^2h/dx^2 which is negative for the type I′ (dh/dx decreases) and is positive for the type I when dh/dx increases except of the short initial section.

The second remark concerns the relation (31), which links the velocity and direction of motion of the front with the thickness of the cold air mass and therefore may be of prognostic significance. We will represent it as a formula for calculating the frontal velocity as follows

$$c = u_g - |V_g| \frac{\cos\beta}{h_1} \times [\cos(\alpha+\beta) - e^{-h_1}\cos(\alpha+\beta+h_1)], \qquad (34)$$

where, h_1, u_g and V_g are dimensionless variables scaled as shown in Table 1, c is defined by (14) and β is defined by (20), (14) and (8). Since $h_1 > 2$ in almost all the cases, this formula can be simplified without a significant loss of accuracy as

$$c = u_g - |V_g| \frac{\cos\beta}{h_1}\cos(\alpha+\beta). \qquad (35)$$

Some difficulties arose, when we tried to check its validity on the basis of observations, because of the lack of all needed observational data (frontal speed, upper level geostrophic wind speed, and the inversion position). In addition, many studies do not concern an identification of the frontal type on the basis of the temperature and wind fields while it is important to identify a case as a katafront before applying eq. (31). Three case-studies, in which it is safe to say that we deal with a katafront, are brought together in Table 2. The results look encouraging from the point of view of both absolute values and a tendency.

4. Discussion

The results of our calculations and qualitative comparison of the theory with the published observations and conceptual models of mature fronts give ground to conclude that the proposed theoretical model incorporates the basic physical relations determining the process of a steady propagation of two air masses of different temperatures. Different frontal features pointed out in separate observational studies (such as a rearward ascending flow in a warm air mass above the front or a warm air ascent ahead of the surface front, a transition from ascending to descending flow below the front, the horizontal low-level jet stream in the warm air mass, the vertical velocity maximum near the surface, the position and slope of

Table 2. *Comparison of observed front velocities with those predicted by the model*

	u_g (m/s)	v_g (m/s)	α (rad)	h_f (km)	h_1	c (m/s)	c' (m/s)	c_f (m/s)
MS	**11**	**15**	−0.9	**∼2**	2.6	8.3	8.5	**6**
S	**16**	**16.7**	−0.8	**∼3**	3.9	14.0	14.0	**12**
T	**13**	**14**	−0.8	**∼2**	2.6	10.3	10.5	**8**

Observational data was taken from the case studies of cold katafronts by Moor and Smith (1989), Sansom (1951) and Testud et al. (1980), (abbreviated as MS, S and T, respectively). Observed values (bold): u_g, v_g: upper level wind components relative to the front; h_f: the approximate frontal height estimated on the base of observations; c_f: the velocity of the front. Calculated values: $\alpha = -\arctan(u_g/v_g)$, h_1: dimensionless height of the front; c and c': predicted frontal velocities defined by (34) and (35) respectively, with $K = 30\ m^2\ s^{-1}$, $f = 10^{-4}\ s^{-1}$, $g = 10\ m\ s^{-1}$, $\beta = 1.2$.

the inversion zone as well as a change in curvature of isobars towards to the front and so on) are reproduced by the theory. However the theory not simply reproduces the frontal features it also indicates the conditions under which these frontal features can occur and thus permits to connect seemingly unconnected observational information and make some predictions. An analytical form of the solution enables one to extract the basic parameters determining the frontal motion in a mature frontal system. The analysis of the results shows that evidently all the dynamic factors involved in the model (in particular, the turbulent friction and the surface friction) are necessary for reproducing and explanation of the frontal features. It also shows that the model of a mature front excluding frontogenetic forcing effects is sufficient for explaining many frontal features found in observations of fully developed fronts.

Several points need to be addressed for a more complete exposition of the subject.

Analysis of the solution shows that assumption of a constant vertical turbulent coefficient requires allowance for the surface layer (even though in the first approximation as it is in our work) to avoid inconsistencies. A study of the behavior of the solution in the vicinity of the surface front (see Appendix) displays some of the inconsistencies. In the case of $\beta = \pi/4$ (the surface layer is absent), the horizontal wind component normal to the front does not coincide with the velocity of the front at the line $x = 0$, $z = 0$; this contradiction disappears when the surface layer is introduced into the problem. Similarly, the calculation of the vertical velocity in the vicinity of the surface front in the case of $\beta = \pi/4$ yields infinity instead of finite quantity when the surface layer is present. So it seems that there is a flaw in the formulation of the problem incorporating the K-model of turbulence, if the no-slip condition at the earth's surface is used.

The inertial forces are not included into a force balance on the front because of the linearization made in the initial equations. However, having the solution obtained, one can estimate the order of the neglected terms retrospectively using the wind velocity fields found. The absolute value of the ratio $u(dv/dx)/fu$ (it is $\frac{2}{3}u(dv/dx)/u$ in dimensionless variables, see scales in Table 1) can be chosen as a measure of the relative magnitude of the nonlinear terms. The selected isolines of this quantity for two main types of cold fronts are drawn in Figs. 5a and 5b by dashed lines. The nonlinear terms appear to be quite small for the katafront solution. For the anafront solution their relative magnitude in the region, the most important from the observational point of view, does not exceed the value 0.6, which is considered to be quite admissible in practice of applications of asymptotic methods.

In spite of a large number of published works on fronts, there appear to be very few published statistics on frontal characteristics. We can mention only that by Sansom (1951) and the works containing confirmation of some of Sansom's results, as, for example, Miles (1962), and also the works trying to confirm some formulae of gravity current models — see Smith and Reeder (1988). Reasoning for that is seemingly a lack of a theoretical basis for defining parameters significant for the front behavior. One of the purposes of such an analytical model as ours is to draw attention to the parameters, which could be important for a classification of mature steady-state fronts. After

Sansom (1951), the difference of the frontal speed and the front-normal high-level wind speed is used for distinguishing between two types of cold fronts (Moor and Smith 1989). Sansom (1951) reported that anafronts mostly occur when the front propagates faster than the geostrophic wind (i.e., $u_g < c$) and katafronts occur when $u_g > c$. Thus, only the sign of the difference $u_g - c$ plays a part in Sansom's classification. Our results extend and enrich Sansom's classification. First, the angle α between the front velocity and geostrophic wind is involved in the classification and the limits of Sansom's sign criterion in distinguishing between two types of fronts are defined. In particular, this sign criterion (depending on the sign of A in our terms) loses its validity for the fronts with rather large negative values of v_g (large values of γ in Fig.2). Secondly, now the value of A coupled with the value of the second parameter γ defines the conditions for all types of fronts (cold, warm, ana-, kata-) to exist. In particular, in accordance with (29) cold fronts can exist only for the values of A not exceeding a limiting value $\sin\gamma + \cos\gamma$. Referring to the basic physical sense of the parameters A and γ discussed above, one can say that there is a limiting value of a difference $u_g - c$ for cold fronts to exist which depends on the angle α between the front velocity and geostrophic wind vectors. For example, cold fronds, propagating approximately in the direction of the geostrophic wind (α is close to zero, $\gamma \approx 1.2$), can not have a speed less than $c \approx 2/3 u_g$ ($A \sim 1$ so that $(u_g - c)/u_g \sim \cos\beta \approx 1/3$). To check this and other predictions of the theory a statistical data on front characteristics are needed.

5. Acknowledgments

The authors are grateful to the reviewers for their helpful comments and suggestions that contributed significantly to the improvement of this paper.

6. Appendix

Behavior of the solution in the vicinity of the surface front

To consider the behavior of the solution in a region close to the singularity along the surface front, where $h = 0$ and $|\mathrm{d}h/\mathrm{d}x| = \infty$, we shall find a value of u_j ($j = 1, 2$) at this line using (18), (19) and (29). After some transformations we obtain:

$$u_j\Big|_{\substack{z=0\\h\to 0}} = u_j\Big|_{\substack{z=h\\h\to 0}} = u_2\Big|_{\substack{h=0\\z\to 0}} = c. \tag{A1}$$

One can see that approaching the singularity by three different ways, we arrive at the same result: along the surface front, where the front is vertical, the horizontal wind component normal to the front coincides with the velocity of the front. Calculation of w_j in the vicinity of the surface front by the formulae (18), (19) and (22), in the case of approaching to the surface front along a horizontal, gives $w_j = 0$ which is natural, because the solution of the problem satisfies the condition (10). Calculations of w_j by the formula (12), i.e., descending to the surface front, give another result. Since the first term in the expansion for $u_1 - C$, calculated from eqs. (18) and (19), is of the order of h, and the first term in the expression (29) for h' is of the order of h^{-1}, the formula (12) after some transformations yields:

$$w_j\Big|_{\substack{z=h\\h\to 0}} = -\frac{\cos^2}{\cos 2\beta}\, a \times \left[\sin\gamma + \left(\sin 2\beta + \cos 2\beta - \frac{1}{3}\right)\frac{a}{2\cos 2\beta}\right]. \tag{A2}$$

According to this formula, vertical velocity w_j on the surface front may be positive, negative or even zero. By analogy with some hydrodynamic problems one can interpret this result as follows. In the vicinity of the surface front in nature, ascending and descending fluxes connected with the front may occur at a height of the order of the surface layer thickness.

In the case of $\beta = \pi/4$ (the surface layer is absent), (29) is replaced by $h' = (-3/2)Ch^{-2}$ and, then, as the result of the passage to the limit $h \to 0$ in (18) and (19), we obtain in (A1) $3c/2$ instead of c which contradicts formulation of the problem (except for the case of $c = 0$). Calculation of the vertical velocity in the vicinity of the surface front in the case of $\beta = \pi/4$ gives for w_j infinity instead of finite quantity (A2), since in this case the main term of the expansion for $u_1 - c$ is finite and the main term of the expansion for h' is of the order of h^{-2}.

REFERENCES

Ball, F. K. 1960. A theory of fronts in relation to surface stress. *Quart. J. Roy. Meteor. Soc.* **86**, 51–66.

Blumen, W. 1980. A comparison between the Hoskins–Bretherton model of frontogenesis and the analysis of an intense surface frontal zone. *J. Atmos. Sci.* **37**, 65–77.

Blumen, W. 1990. A semigeostrophic Eady-Wave Frontal Model Incorporating Momentum diffusion. Part I: Model and Solutions. *J. Atmos. Sci.* **47**, 2890–2902.

Blumen, W. and Wu, R. 1983. Baroclinic instability and frontogenesis with Ekman boundary layer dynamics incorporating the geostrophic momentum approximation. *J. Atmos. Sci.* **40**, 2630–2637.

Browning, K. L. 1986. Conceptual models of precipitation systems. *Wea. Forecasting* 1, 23–41.

Browning, K. L. and Harrold, T. W. 1969. Air motion and precipitation growth in a wave depression. *Quart. J. Roy. Meteor. Soc.* **95**, 288–309.

Browning, K. A., Harrold, T. W. and Starr, J. R. 1970. Richardson number limited shear zones in the free atmosphere. *Quart. J. Roy. Meteor. Soc.* **96**, 40–49.

Browning, K. L. and Pardoe, C. W. 1973. Structure of low-level jet streams ahead of midlatitude cold fronts. *Quart. J. Roy. Meteor. Soc.* **99**, 369–389.

Egger, J. 1988. Frictionally induced circulations in fronts. *Beitr. Phys. Atmosph.* **61**, 140–142.

Eliassen, A. 1948. The quasi-static equations of motion. *Geofys. Publikasjoner* **17** (no. 3), 277–287.

Eliassen, A. 1959. On the formation of fronts in the atmosphere. *The atmosphere and the sea in motion.* New York: Rockefeller Institute Press, pp. 277–287.

Eliassen, A. 1962. On the vertical circulation in frontal zones. *Geofys. Publikasjoner* **24** (no. 4), 147–160.

Emanuel, K. A. 1985. Frontal circulations in the presence of small moist symmetric instability. *J. Atmos. Sci.* **42**, 1062–1071.

Emanuel, K. A., Fantini, M. and Thorpe, A. J. 1987. Baroclinic instability in an environment of small stability to slantwise convection. Part I: Two-dimensional models. *J. Atmos. Sci.* **44**, 1559–1573.

Gutman, L. N. 1972. *Introduction to the nonlinear theory of mesoscale meteorological processes.* Israel Program for Scientific Translations. Jerusalem. 224 pp.

Gutman, L. N. and Mal'ko, L. N. 1961. On the theory of fronts. *Proc.* (Doklady) *Acad. Sci. USSR* **138**, 622–624.

Hoskins, B. J. 1982. The mathematical theory of frontogenesis. *Ann. Rev. Fluid Mech.* **14**, 131–151.

Hoskins, B. J. and Bretherton, F. P. 1972. Atmospheric frontogenesis models: Mathematical formulation and solution. *J. Atmos. Sci.* **29**, 11–37.

Hoskins, B. J. and West, N. V. 1979. Baroclinic waves and frontogenesis. Part II: Uniform potential vorticity jet flows. Cold and Warm fronts. *J. Atmos. Sci.* **36**, 1663–1680.

Kalazhokov, Kh. Kh. and Gutman, L. N. 1964. On the dynamic structure of fronts. *Bull.* (Isvestiya) *Acad. Sci. USSR, Geophys. Ser.* **1**, 136–149.

Keyser, D. and R. A. Anthes, 1982. The influence of planetary boundary layer physics on frontal structure in the Hoskins–Bretherton horizontal shear model. *J. Atmos. Sci.* **39**, 1783–1802.

Manton, M. J. 1981. On the propagation of cold fronts. *Quart. J. Roy. Meteor. Soc.* **107**, 875–882.

Manton, M. J. 1985. On the classification of cold fronts. *Contrib. Atmos. Phys.* **58**, 100–116.

Margules, M. 1906. Uber temperaturaturschichtung in stationar bewegtter und in ruhender luft (On the temperature stratification in steady moving and calm air). *Hann-Band. Meteor. Z.* 243–254.

Miles, M. K. 1962. Wind, temperature and humidity distribution at some cold fronts over SE England. *Quart. J. Roy. Meteor. Soc.* **88**, 260–300.

Moor, J. T. and Smith, K. F. 1989. Diagnosis of anafronts and katafronts. *Wea. Forecasting* **4**, 61–72.

Ogura, Y. and Portis, D. 1982. Structure of the cold front observed in SESAME-AVE III and its comparison with the Hoskins–Bretherton frontogenesis model. *J. Atmos. Sci.* **39**, 2773–2792.

Orlanski, I., Ross, B., Polinsky, L. and Shaginaw, R. 1985. Advances in the theory of atmospheric fronts. *Advances in Geophysics* **28B**, 223–252.

Panofsky, H. A. and Dutton, J. A. 1984. *Atmospheric turbulence.* Wiley, 397 pp.

Rao, G. V. 1971. A numerical study of frontal circulation in the atmospheric boundary layer. *J. Appl. Meteor.* **10**, 26–35.

Sanders, F., 1955. An investigation of the structure and dynamics of an intense surface frontal zone. *J. Meteor.* **12**, 542–552.

Sansom, H. W. 1951. A study of cold fronts over the British Isles. *Quart. J. Roy. Meteor. Soc.* **77**, 96–120.

Sawyer, J. S. 1956. The vertical circulation in meteorological fronts and its relation to frontogenesis. *Proc. R. Soc.* London Ser. A, **234**, 346–362.

Simpson, J. E. 1982. Gravity currents in the laboratory, atmosphere and ocean. *Ann. Rev. Fluid Mech.* **14**, 213–234.

Smith, R. K. and Reeder, M. J. 1988. On the movement and low-level structure of cold fronts. *Mon. Wea. Rev.* **116**, 1927–1944.

Testud, J., Breger, G., Amayenc, P., Chong, M., Nutten, B. and Sauvaget, A. 1980. A Doppler radar observation of a cold front: three dimensional air circulation, related precipitation system and associated wavelike motion. *J. Atmos. Sci.* **37**, 78–98.

Thompson, W. T. and Williams, R. T. 1997. Numerical simulations of maritime frontogenesis. *J. Atmos. Sci.* **54**, 314–331.

Thorpe, A. J. and K. A. Emanuel, 1985. Frontogenesis in the presence of small stability to slantwise convection. *J. Atmos. Sci.* **42**, 1809–1824.

Welander, P. 1963. Steady plane fronts in a rotating fluid. *Tellus* **15**, 34–43.

Williams, R. T. 1967. Atmospheric frontogenesis: A numerical experiment. *J. Atmos. Sci.* **24**, 627–641.

Williams, R. T. 1972. Quasi-geostrophic versus non-geostrophic frontogenesis. *J. Atmos. Sci.* **29**, 3–10.

Williams, R. T. 1974. Numerical simulation of steady-state fronts. *J. Atmos. Sci.* **31**, 1286–1296.